Smooth self-similar imploding profiles to 3D compressible Euler

This review article is dedicated to Constantine Dafermos' 80th birthday

Tristan Buckmaster*, Gonzalo Cao-Labora† and Javier Gómez-Serrano‡

Abstract

The aim of this note is to present the recent results in [7], concerning the existence of "imploding singularities" for the 3D isentropic compressible Euler and Navier-Stokes equations. Our work builds upon the pioneering work of Merle, Raphaël, Rodnianski and Szeftel [46, 47, 45] and proves the existence of self-similar profiles for all adiabatic exponents $\gamma > 1$ in the case of Euler; as well as proving asymptotic self-similar blow-up for $\gamma = \frac{7}{5}$ in the case of Navier-Stokes. Importantly, for the Navier-Stokes equation, the solution is constructed to have density bounded away from zero and constant at infinity, the first example of blow-up in such a setting. For simplicity, we will focus our exposition on the compressible Euler equations.

1 Introduction

The compressible Euler equations describe the conservation of mass, momentum, and energy in a fluid, and are important in many fields, including aerodynamics and astrophysics. In this review, we present recent developments regarding the existence of smooth imploding solutions for the compressible Euler equations. The full compressible Euler equations take the form

$$\partial_t(\rho \ u) + \operatorname{div}(\rho u \otimes u + p \ \operatorname{Id}) = 0$$

$$\partial_t \rho + \operatorname{div}(\rho u) = 0$$

$$\partial_t E + \operatorname{div}((p + E)u) = 0$$

where u is the velocity, ρ is the density, p is the pressure, and E is the energy. The equations describe the conservation of momentum, mass, and energy in a fluid, respectively. The pressure is given by the ideal gas law

$$p = (\gamma - 1)(E - \frac{1}{2}\rho |u|^2) = \frac{1}{\gamma}\rho^{\gamma}e^S,$$

for the adiabatic exponent $\gamma > 1$. The sound speed is given by $c = \sqrt{\frac{\gamma p}{\rho}}$.

^{*}Department of Mathematics, University of Maryland, College Park, MD tristanb@umd.edu

[†]Department of Mathematics, Massachusetts Institute of Technology, Cambridge, MA gcaol@mit.edu

[‡]Department of Mathematics, Brown University, Providence RI javier_gomez_serrano@brown.edu

1.1 Shock waves

Before discussing implosion in detail, let us first describe the classical problem of shock waves, which can be seen as a prototypical singularity in the context of Euler's equations. A shock wave occurs when the speed of a disturbance exceeds the local speed of sound. A fundamental problem in the the mathematical theory of compressible fluids is to provide a complete description of shock formation and development. In particular, one is interested in a complete description of the evolution of a smooth solution up until the point of singularity, and the shock, a co-dimension 1 space-time hypersurface, that proceeds the initial singularity.

The earliest rigorous result regarding shock wave formation traces back to the work of Lax [39] in the 1D setting. Generalizations and improvements of Lax's result were obtained by John [36] and Liu [41], for the 1D Euler equations. See the book of Dafermos [23] for a more extensive bibliography of 1D results.

Sideris [52] proved the existence of finite time singularities in 2D and 3D. The result of Sideris proves that a singularity occurs; however, it is not ascertained what form such a singularity takes. Christodoulou [18] and Christodoulou-Miao [21] demonstrated the formation of shocks for 3D isentropic, irrotational fluids in the relativistic and non-relativistic settings respectively. Luk and Speck built on this work to handle the case of shock formation for 2D isentropic fluids with non-trivial vorticity [42]. The first author, together with Shkoller, and Vicol, employing a different approach, resolved the shock formation problem in the most general setting of full 3D compressible Euler [11, 12] (cf. [43]). The work [11, 12], together with the prior work [10] of the same authors were the first to isolate the self-similar profile of the initial singularity that precedes the development of shock waves. In particular, the works demonstrated that the asymptotic self-similar profile of the singularity is described by self-similar solutions to the Burgers' equation. More recently, Abbrescia and Speck [1] and Shkoller and Vicol [51] have studied the problem of maximal development of shock waves.

With regards to shock development in one spatial dimension, global unique weak solutions satisfying the Rankine-Hugoniot conditions have been established (see [31, 25, 5, 6]), but these methods neither provide a precise description of the shock front nor detect weak discontinuities: characteristic surfaces conjectured by Landau and Lifshitz [38]. In multiple dimensions, Majda [44] studied the short-time evolution of the shock front starting from discontinuous initial data, which is smooth on either side of the shock front. This framework does not cover the shock development problem, where one must evolve from Hölder continuous pre-shock data and weak discontinuities may form. For the one-dimensional p-system (which models 1D isentropic Euler), Lebaud [40] was the first to prove shock formation and development in her thesis work (cf. [16, 37]). In the case of the non-isentropic 3×3 Euler equations in spherical symmetry, shock formation and development were first established by Yin [58]. Independently, Christodoulou and Lisibach [20] demonstrated shock development for the barotropic Euler equations in spherical symmetry. The use of the isentropic model or the assumption of irrotational flow in higher dimensions has been referred to as restricted shock development because it cannot produce weak solutions to the Euler equations. Christodoulou [19] has also established restricted shock development for the irrotational and isentropic Euler equations in three dimensions outside of symmetry.

In [9], the first author, Drivas, Shkoller and Vicol consider the shock development problem for 2D compressible Euler under azimuthal symmetry (see [8] for a recent review article). The work provides

the first full description of shock development; in particular, in addition to describing the shock front, [9] gives the first detailed description of the weak discontinuities of Landau and Lifshitz [38] (see Figure 1).



Figure 1: The image represents the density restricted to the annular region $r \in [1, 2]$. The first image is of the initial data, the second is the preshock, and the third is of the developed shock. The red, green and blue curves represent the shock curve, weak rarefaction wave and weak contact discontinuity respectively.

1.2 Implosion

While shock waves are a common and potentially the only stable form of singularity for the Euler equations, other types of singularities can arise from smooth initial data. It is a fundamentally interesting problem to classify these forms of singularities, both from a mathematics and physics perspective.

Guderley's classical work [34] (cf. [17, 53]) constructed the first examples of non-smooth imploding solutions. Very recently, Merle, Raphaël, Rodnianski, and Szeftel rigorously proved the existence of *smooth* radially symmetric imploding solutions to the isentropic compressible Euler equations [46]:

$$\partial_t(\rho u) + \operatorname{div}(\rho u \otimes u) + \nabla p(\rho) = 0,$$

$$\partial_t \rho + \operatorname{div}(\rho u) = 0,$$
(1.1)

where here $p(\rho) = \frac{1}{\gamma}\rho^{\gamma}$ for $\gamma > 1$. Specifically, for almost every $\gamma > 1$, they showed the existence of a countably infinite sequence of self-similar solutions to (1.1). These solutions exhibit blow-up of both the velocity and density at the origin. The condition on γ is related to the non-vanishing of an analytic function. The case $\gamma = 5/3$, which describes monatomic gases, is specifically ruled out.

The form of the singularity discovered in [46] is fundamentally new. The authors also used these solutions to prove finite-time blow-up for the defocusing, supercritical, nonlinear Schrödinger equation [45], solving a significant open problem in the field. Additionally, the solutions were used as a basis to construct asymptotically self-similar solutions to the three-dimensional isentropic compressible Navier-Stokes equations with density-independent viscosity [47], given by

$$\partial_t(\rho u) + \operatorname{div}(\rho u \otimes u) + \nabla p(\rho) - \mu_1 \Delta u - (\mu_1 + \mu_2) \nabla \operatorname{div} u = 0,$$

$$\partial_t \rho + \operatorname{div}(\rho u) = 0,$$
(1.2)

where (μ_1, μ_2) are the Lamé viscosity coefficients, with $\mu_1 > 0$ and $2\mu_1 + \mu_2 > 0$. Prior to this result, Xin [57] showed the existence of blow-up solutions for initial data with compact density, and Rozanova [50] demonstrated the existence of blow-up solutions for rapidly (polinomially) decaying density. Unlike [47], neither [57] nor [50] provide a description of the singularity that occurs. The result [47] further weakens the decay required on the density leading to singularity formation. To rule out the role of vacuum at spatial infinity in the singularity formation, one however would prefer such solutions to be constructed from initial data that has non-vanishing, constant density at infinity. See also the recent numerical work by Biasi [4].

The papers [46] and [47] left open two fundamental questions:

- 1. Do imploding solutions for the Euler equations exist for any value of γ greater than 1?
- 2. Is it possible to create imploding solutions to the Navier-Stokes equation with an initial density that is constant at infinity?

In [7], we resolved both of these questions. We showed that for all $\gamma > 1$ there exist self-similar imploding solutions. For the case of diatomic gases, $\gamma = \frac{7}{5}$, we showed there exists an infinite sequence of self-similar imploding solutions. The paper [7] also provides simplified proofs of linear stability and non-linear stability, leading to the proof of asymptotically self-similar imploding solutions to the Navier-Stokes equations for $\gamma = \frac{7}{5}$. The initial data for such solutions are chosen to have constant non-zero density at infinity – the first example of such initial data leading to blow-up for the Navier-Stokes equations. The focus of this article will be on the former result.

2 Reduction to an autonomous ODE

Let us rewrite (1.1) in radial form:

$$\partial_t u + u \partial_R u + \frac{1}{\gamma \rho} \partial_R \rho^{\gamma} = 0 \quad \text{and} \quad \partial_t \rho + \frac{1}{R^2} \partial_R (R^2 \rho u) = 0,$$
 (2.1)

where for matters of simplicity, we restricted the problem to three dimensions. Letting $\alpha = \frac{\gamma - 1}{2}$, we define the rescaled sound speed: $\sigma = \frac{1}{\alpha} \rho^{\alpha}$. Then, we make the following self-similar anzatz

$$u(R,t) = r^{-1} \tfrac{R}{T-t} U(\log(\tfrac{R}{(T-t)^{\frac{1}{r}}})) \quad \text{and} \quad \sigma(R,t) = \alpha^{-\frac{1}{2}} r^{-1} \tfrac{R}{T-t} S(\log(\tfrac{R}{(T-t)^{\frac{1}{r}}})) \,,$$

where here r is a self-similar scaling parameter to be determined. Defining the self-similar variable $\xi = \log(\frac{R}{(T-t)^{\frac{1}{r}}})$, then (2.1) reduces to an autonomous system of the form

$$\frac{dU}{d\xi} = \frac{N_U(U,S)}{D(U,S)}, \quad \text{and} \quad \frac{dS}{d\xi} = \frac{N_S(U,S)}{D(U,S)}. \tag{2.2}$$

For, $\gamma = \frac{7}{5}$ and r = 1.079404, the phase portrait is shown in Figure 2, where D, N_U , and N_S are represented by red, green, and black curves, respectively. The point labeled P_s is a special type of singular point for the dynamic system described in equation (2.2). There are two smooth integral curves that pass through P_s , one tangent to the direction ν_- and the other tangent to ν_+ . The curve that is tangent to ν_+ corresponds to the Guderley solution, while the curve tangent to ν_- corresponds to the solution found in [46]. To create

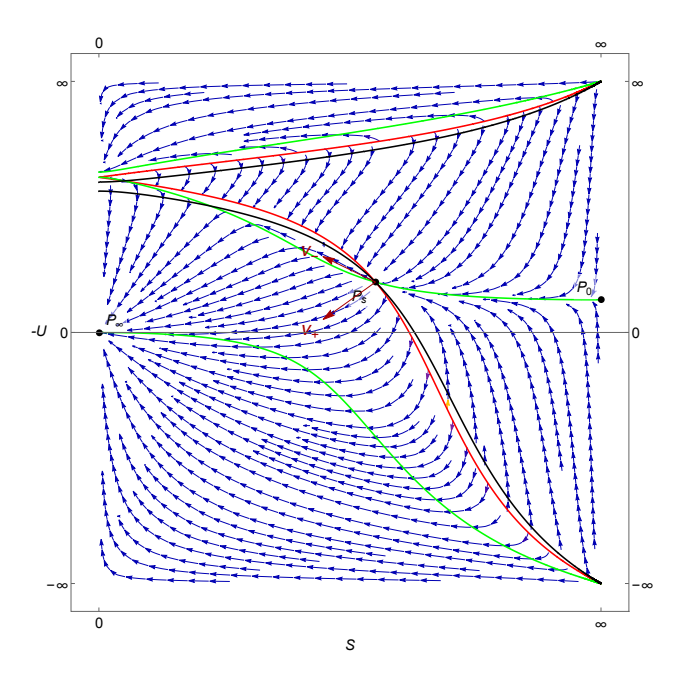


Figure 2: Imploding solutions in (U, S) variables. Note that a singular coordinate change has been made in order to compactify the (U, S) coordinates.

a globally defined self-similar solution, we need to find an integral curve that connects the points P_0 and P_{∞} through P_s . It is not possible to do this using a continuous integral curve with the Guderley solution. However, by introducing a shock discontinuity, we can jump from one point in the phase portrait to another and create a globally defined self-similar solution. In [46], by means of choosing distinguished values of the self-similar scaling parameter r, the authors overcame the challenge that the smooth integral curve tangent to ν_- generally does not connect P_0 to P_{∞} , but rather intersects the sonic line D=0 at a point other than P_s , resulting in a solution that is not globally defined.

Motivated by the works [10, 11, 12], it is helpful to rewrite the system in terms of its Riemann invariants

$$w = u + \sigma \quad \text{and} \quad z = u - \sigma$$
 (2.3)

so that

$$u = \frac{w+z}{2}$$
 and $\sigma = \frac{w-z}{2}$.

One can now diagonalize (2.1) in terms of w and z, in order to rewrite (2.1) as a nonlinear transport equation

$$\partial_t w + \frac{1}{2} (w + z + \alpha (w - z)) \partial_R w + \frac{\alpha}{2R} (w^2 - z^2) = 0$$

$$\partial_t z + \frac{1}{2} (w + z - \alpha (w - z)) \partial_R z - \frac{\alpha}{2R} (w^2 - z^2) = 0.$$
(2.4)

Employing the self-similar ansatz

$$w(R,t) = \frac{1}{r} \cdot \frac{R}{T-t} W(\xi) \quad \text{and} \quad z(R,t) = \frac{1}{r} \cdot \frac{R}{T-t} Z(\xi)$$

$$(2.5)$$

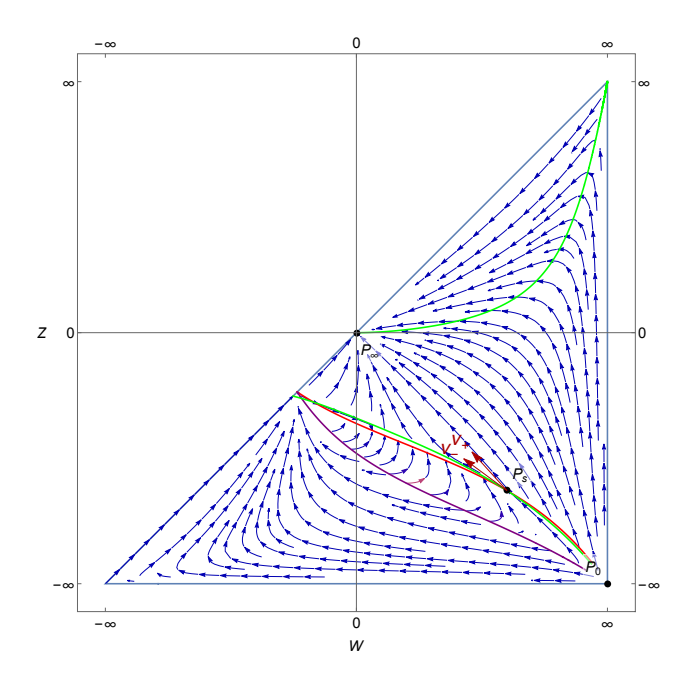


Figure 3: Imploding solutions in (W, Z) variables. Note that a singular coordinate change has been made in order to compactify the (W, Z) coordinates.

where we recall $\xi = \log(\frac{R}{(T-t)^{\frac{1}{r}}})$, then we obtain

$$(r + \frac{1}{2}((1+2\alpha)W + (1-\alpha)Z))W + (1 + \frac{1}{2}(W + Z + \alpha(W - Z)))\partial_{\xi}W - \frac{\alpha}{2}Z^{2} = 0$$

$$(r + \frac{1}{2}((1-\alpha)W + (1+2\alpha)Z))Z + (1 + \frac{1}{2}(W + Z - \alpha(W - Z)))\partial_{\xi}Z - \frac{\alpha}{2}W^{2} = 0$$
(2.6)

Rearranging, we obtain the autonomous system

$$\partial_{\xi}W = \frac{-(r + \frac{1}{2}((1 + 2\alpha)W + (1 - \alpha)Z))W + \frac{\alpha}{2}Z^{2}}{1 + \frac{1}{2}(W + Z + \alpha(W - Z))} = \frac{N_{W}}{D_{W}},$$

$$\partial_{\xi}Z = \frac{-(r + \frac{1}{2}((1 - \alpha)W + (1 + 2\alpha)Z))Z + \frac{\alpha}{2}W^{2}}{1 + \frac{1}{2}(W + Z - \alpha(W - Z))} = \frac{N_{Z}}{D_{Z}}.$$
(2.7)

In Figure 3, the phase portrait for the region where the density is positive (W - Z > 0) is shown. The red, purple, and green lines represent $D_Z = 0$, $D_W = 0$, and $N_Z = 0$, respectively. One key difference between this system and (2.2) is that the denominator D_W does not vanish at the point P_s , which simplifies the analysis in the area around P_s . The variables (W, Z) provide a geometric understanding of the imploding solution in terms of the trajectories of the W and Z waves. P_s is an unstable fixed point for the trajectories of Z-waves and divides space into an interior region (the backward acoustic cone emanating from the singular point) and an exterior region. Z-waves in the exterior region cannot enter the interior region, while Z-waves in the interior region cross the origin to become W-waves, then cross P_s and travel to the exterior region. Since the system in (2.7) is autonomous, we can choose the location $\xi = 0$ to be where the solution crosses P_s .

The key steps to constructing a smooth integral curve from P_0 to P_∞ are:

- 1. Apply a careful local analysis of the behavior of the smooth solution tangent to ν_{-} . In particular, show that the solutions wiggle in a certain manner with a continuous change in the self-similar parameter r.
- 2. Demonstrate that such a wiggling phenomenon combined with barrier arguments and continuity leads to a smooth solution connecting P_0 and P_{∞} .

3 Local analysis of P_s

To better understand P_s , we can recast the system using the variable $\xi \mapsto \psi$, where $\partial_{\psi} = D_W D_Z \partial_{\xi}$. For simplicity, let us focus on the case where $\gamma = \frac{5}{3}$. We obtain the ODE:

$$\partial_{\psi}W = -\frac{1}{18}(3+W+2Z)(6rW+5W^2+2WZ-Z^2) \quad \text{and} \quad \partial_{\psi}Z = \frac{1}{18}(3+2W+Z)(W^2-2(3r+W)Z-5Z^2),$$
(3.1)

for which P_s is a stable stationary point. Let $0 < \lambda_- < \lambda_+$ be the eigenvalues of the resulting system of the Jacobian matrix at P_s . We let k denote the ratio of the two eigenvalues:

$$k = \frac{\lambda_{-}}{\lambda_{+}} = \frac{r - 2 - \sqrt{2r - 2}}{r - 2 + \sqrt{2r - 2}}.$$
(3.2)

The directions ν_{-} and ν_{+} defined earlier (the directions of the two smooth integral curves passing through P_s) are also the eigenvectors of the Jacobian of (3.1) that correspond to the eigenvalues λ_{-} and λ_{+} respectively. We will focus on the smooth solutions of (2.7) that have tangents parallel to ν_{-} . These two directions are shown in Figure 3.

In the range $1 < r < r^* (= 3 - \sqrt{3} \text{ for } \gamma = \frac{5}{3})$, k is a monotonically increasing function of r that approaches infinity as r approaches r^* . The smooth solution passing through point P_s can be expressed as a Taylor series around $\xi = 0$ in the form $(W(\xi), Z(\xi)) = \sum_{n=0}^{\infty} \frac{\xi^n}{n!} (W_n, Z_n)$. The Taylor coefficients of $D_{\circ}(W, Z)$ and $N_{\circ}(W, Z)$ are denoted by $D_{\circ,n}$ and $N_{\circ,n}$, respectively. For $n \ge 2$, the following equations hold:

$$D_{W,0}W_n = N_{W,n-1} - \sum_{j=0}^{n-2} {n-1 \choose j} D_{W,n-1-j} W_{j+1},$$

$$Z_n D_{Z,1}(n-k) = -\sum_{j=1}^{n-2} {n \choose j} D_{Z,n-j} Z_{j+1} + (N_{Z,n} - (\partial_Z N_Z(P_2)) Z_n) + Z_1 (-D_{Z,n} + Z_n \partial_Z D_Z(P_2)).$$
(3.3)

By choosing (W_1, Z_1) to align with ν_- , these equations can be used to iteratively solve for a power series that describes the smooth solution tangent to ν_- at P_s in a small neighborhood of P_s . Note that the right-hand side of the second equation does not depend on Z_n .

For any positive integer j, we define r_j such that $j = k(r_j)$. It can be observed the expression for Z_n in (3.3) becomes singular as k(r) approaches n and changes sign at k(r) = n. This causes the integral curve of the smooth solution to exhibit a wiggling effect, which allows us to show that for $\gamma > 1$ and n = 3:

- 1. For $r \in (r_n, r_{n+1})$, the solution to the left of P_s approaches P_{∞} as ξ goes to infinity.
- 2. For $r = r_n + \varepsilon$, the solution to the right of P_s intersects the line $D_W = 0$.

¹We believe this is true for all $\gamma > 1$ and every odd n.

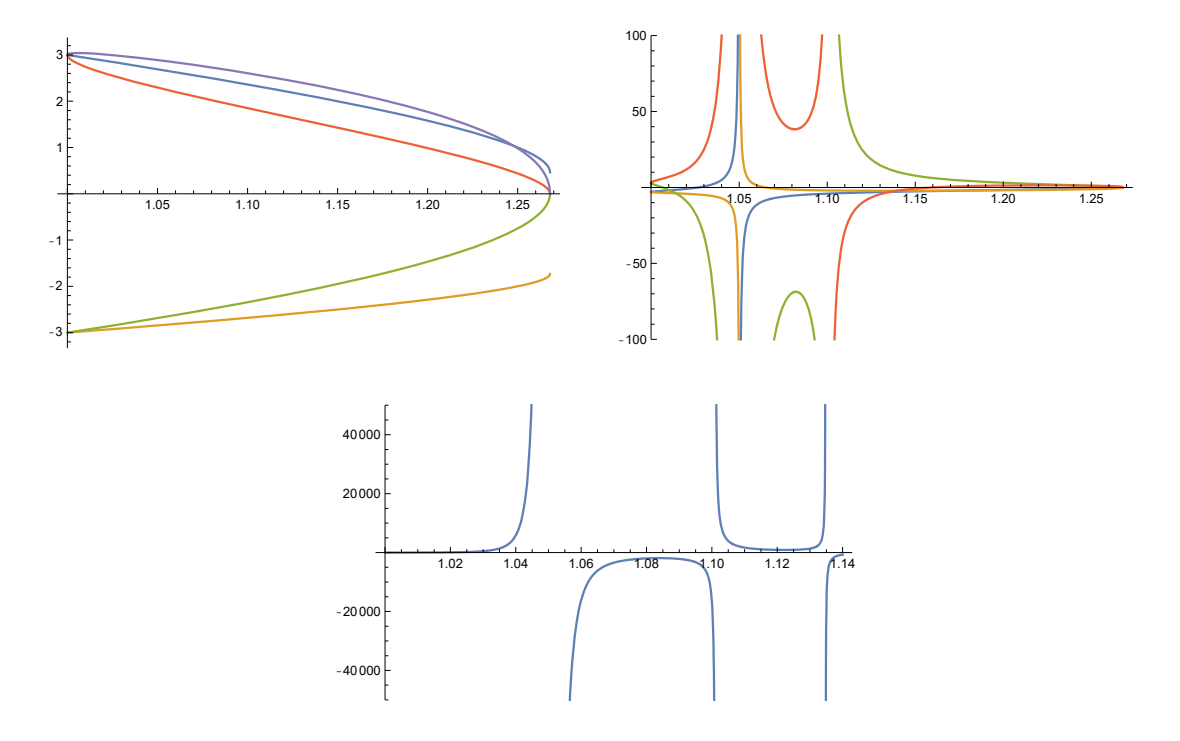


Figure 4: In the first plot, we show W_0 (blue), Z_0 (orange), W_1 (green), Z_1 (red) and W_2 magenta. In the second plot, we show Z_2 (blue), W_3 (orange), Z_3 (green) and W_4 (red). In the last plot, we show Z_4 . The singularities happen at $r = r_2 = 11 - 3\sqrt{11} \approx 1.05013$, $r = r_3 = 6 - 2\sqrt{6} \approx 1.10102$ and $r = r_4 = \frac{1}{6}(43 - 5\sqrt{43}) \approx 1.13476$.

3. For $r = r_{n+1} - \varepsilon$, the solution to the right of P_s intersects the line $D_Z = 0$.

If we can demonstrate points 2 and 3, then using a simple shooting argument, we can conclude that there exists an r within the range (r_n, r_{n+1}) such that the solution curve connects P_s to P_0 . Additionally, point 1 implies that the solution curve also connects P_s to P_{∞} .

We have plotted the coefficients $\{W_i, Z_i\}_{i=0}^4$ for $r \in (1, r^*)$ in Figure 4. Note that at $r \approx r_n$ the singularity of Z_n will propagate to every W_i, Z_i for i > n since they depend on Z_n via the recurrence (3.3).

4 Barrier arguments

For the sake of simplicity, let us concentrate on how to show items 1, 2 and 3 for the case $\gamma = \frac{5}{3}$ and $k \in (3, 4)$, which corresponds to $r \in (r_3, r_4)$.

The idea to prove item 1 is to construct two different barriers bounding the behavior of the solution. We will have one global barrier which we denote by $b^{fl}(t)$ and a local one, which we denote by $b^{nl}(t)$. They are given by

$$b^{\rm nl}(t) = \left(\sum_{i=0}^{3} \frac{W_i}{i!} t^i, \sum_{i=0}^{3} \frac{Z_i}{i!} t^i\right),$$

$$B^{\rm fl}(W, Z) = \left(W_0 + B_1 W_1 t + \frac{B_2}{2} t^2, Z_0 + B_1 Z_1 t + \frac{B_3}{2} t^2\right),$$

where the coefficients B_2 , B_3 are chosen so that $b^{\text{fl}}(1) = P_{\odot}$ and the coefficient B_1 is chosen so that the barrier matches one further order with the ODE at P_{\odot} . The point P_{\odot} is defined as the intersection of $N_W = N_Z = 0$ on the W > Z half-plane. One can see both barriers in Figure 5.

The global barrier will connect the point P_s with P_{\odot} in such a way that all trajectories of the ODE traverse $B^{\rm fl}$ upwards. Once we show that the smooth solution stays above $b^{\rm fl}(t)$ it is easy to conclude it has to converge to P_0 , however, $b^{\rm fl}(t)$ will not be well-adapted to the geometry of the phase portrait at P_s , and this means that the smooth solution will not start above $b^{\rm fl}(t)$. In order to solve that, we use the local barrier $b^{\rm nl}(t)$ which matches the smooth solution up to third order, and thus is well-adapted to the geometry of the phase portrait at P_s . In particular, the smooth solution will start above $b^{\rm nl}(t)$ and trajectories will traverse $b^{\rm nl}(t)$ upwards for a short period of time $t \in [0, t_v]$. Thus, if we show that $b^{\rm nl}(t)$ and $B^{\rm fl}$ intersect at some time $t \in (0, t_v)$, we will be done, since the concatenation of the two barriers will correctly bound the behavior of the solution. This is done via a computer-assisted proof which involves a careful desingularization as $k \to 3^+$.

We now describe how to prove items 2 and 3. Let us consider $n \in \{3,4\}$ and define the local barrier

$$b_n^{\text{nr}}(t) = \left(\sum_{i=0}^n \frac{W_i}{i!} (-t)^i, \sum_{i=0}^n \frac{Z_i}{i!} (-t)^i + \frac{(-1)^n \beta |Z_n|}{(n+1)!} (-t)^{n+1}\right), \quad \text{for } 0 \leqslant t \leqslant \beta |k-n|^{\frac{1}{n-1}}$$

$$(4.1)$$

which matches until n-th order with the smooth solution at P_s . We then define

$$P_n^{\rm nr}(t) = (\partial_{\psi} W(b_n^{\rm nr}(t)), \partial_{\psi} Z(b_n^{\rm nr}(t))) \wedge b_n^{\rm nr}'(t),$$

so that the sign of $P_n^{\text{nr}}(t)$ informs us if the solutions of the ODE are traversing $b_n^{\text{nr}}(t)$ in the upwards direction (negative sign) or in the downwards direction (positive sign). A careful computation of $P_n^{\text{nr}}(t)$ yields

$$P_n^{\rm nr}(t) = \frac{|N_{W,0}D_{Z,1}|\beta}{(n+1)!} |Z_n|(-t)^{n+1} + \frac{|\partial_z D_Z(P_s)N_{W,0}|}{n!(n-1)!} Z_n^2(-t)^{2n-1} + o_{r \to r_n} \left(\beta |Z_n| t^{n+1} + Z_n^2 t^{2n-1}\right)$$
(4.2)

For item 2, we set n=3. Comparing the (n+1)-th Taylor coefficients of (4.1) and the smooth solution, one can see that $b_3^{\rm nr}(t)$ will be above the smooth solution near P_s provided β is chosen sufficiently large. Moreover, from (4.2), the barrier $b_3^{\rm nr}(t)$ will bound the trajectory of the smooth solution up to $t \leq c\beta |k-n|$. We construct another barrier $B^{\rm fr}$ given in implicit form by the nullset of:

$$B^{fr}(W,Z) = (W - W_0 - \frac{1}{2}Z + \frac{1}{2}Z_0)(W + Z - F_0) - F_1(W + Z - W_0 - Z_0).$$

The values of F_0 and F_1 are chosen so that $B^{\rm fr}$ matches the subleading order terms of its Taylor expansion with the smooth solution both at P_0 and P_s . Concretely, $F_0 = -2(r-1)$ and $F_1 = (W_0 + Z_0 - F_0) \frac{Z_1/2 - W_1}{W_1 + Z_1}$. We can define $P_3^{\rm fr}(t)$ in the same way as we defined $P_3^{\rm nr}(t)$ and we show with a computer-assisted proof that $P_3^{\rm fr}(t) > 0$. That is, solutions always traverse $B^{\rm fr}(W, Z) = 0$ downwards. We have plotted $b_3^{\rm nr}(t)$ and $B^{\rm fr}(W, Z) = 0$ in Figure 5.

Finally, we want to show that the concatenation of $b_3^{\text{nr}}(t)$ and B_3^{fr} yields a barrier that bounds adequately the global behavior of the smooth solution. To that end, it suffices to show that both barriers intersect at some time $t_i \in (0, c\beta(k-3))$, so that $b_3^{\text{nr}}(t)$ remains valid up to t_i . The choice of F_0, F_1 guarantees that the Taylor expansions at P_s of $b_3^{\text{nr}}(t)$ and B^{fr} first differ at their second order coefficients. Comparing their

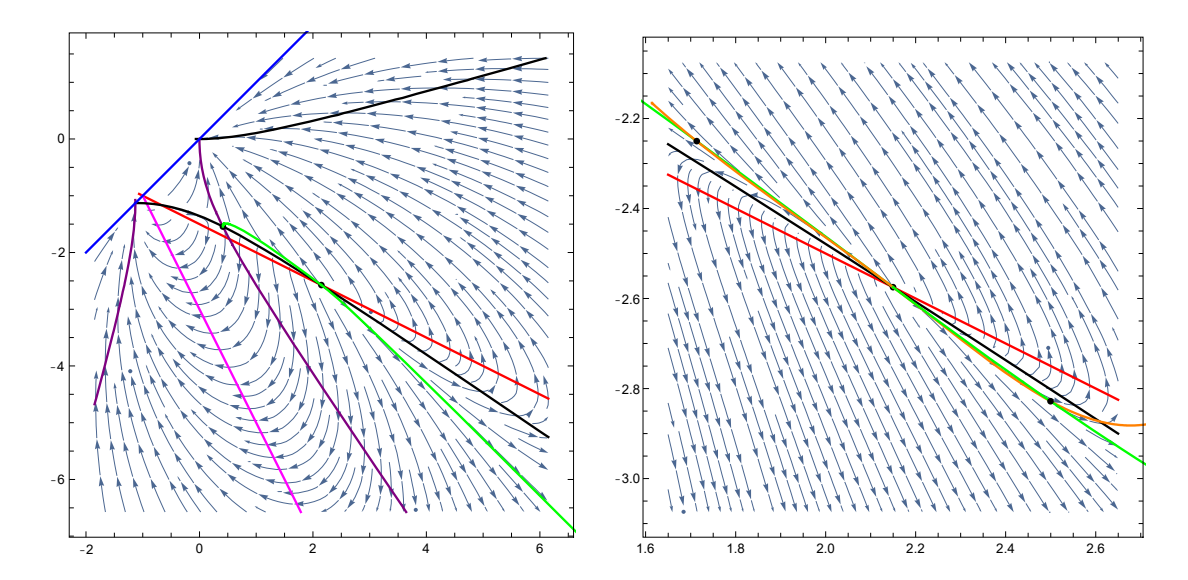


Figure 5: Two plots at different scales of the vector field (W_{ψ}, Z_{ψ}) for $r = 1.13 \in (r_3, r_4)$. In the center we have P_s , which is the intersection of $D_Z = 0$ (red line) and $N_Z = 0$ (black curve). We also show $D_W = 0$ (in pink) and $N_W = 0$ (in purple). In green, we have the global barriers $b^{\text{fl}}(t)$ (to the left of P_s) and $B^{\text{fr}}(W, Z) = 0$ (to the right of P_s). At the smallest scale, we also show in orange the local barriers $b^{\text{nl}}(t)$ (to the left of P_s) and $b_3^{\text{nr}}(t)$ (to the right of P_s). For $b_3^{\text{nr}}(t)$ we took $\beta = 500$. We have also indicated the points of intersection of the local barriers and the global barriers.

Taylor series one can conclude that both barriers intersect at some $t_i \lesssim |k-3|$, so $t_i \leqslant c\beta(k-3)$ taking β sufficiently large.

With respect to item 3, we set n=4 and use the local barrier (4.1). Taking β sufficiently large, $b_4^{\rm nr}(t)$ will be below the smooth solution for t sufficiently small. Moreover, in this case, both terms from (4.2) are negative, giving that solutions to the ODE cross $b_4^{\rm nr}(t)$ upwards for every $0 \le t \le \beta(4-k)^{1/3}$. Therefore, if we show that $b_4^{\rm nr}(t)$ intersects $D_Z = 0$ for some $t < \beta(4-k)^{1/3}$ we will be done. In that interval, we can compute

 $D_Z(b_4^{\rm nr}(t)) = \frac{W_1 + 2Z_1}{3}t + \frac{Z_4}{36}t^4 + o_{k\to 4^-}((4-k)^{2/3}),$

where the two main terms are both of order $(4-k)^{1/3}$. Checking that the two main terms have different signs, we deduce that $b_4^{\rm nr}(t)$ intersects $D_Z = 0$ at some $t \leq \beta (4-k)^{1/3}$, provided that β is chosen sufficiently large. We have a plot of this situation in Figure 6.

5 Computer-assisted proofs

The representation of real numbers using a finite number of zeros and ones has the advantage of allowing finite calculations and a practical framework. However, this method also has the disadvantage of being limited to a finite (although large) amount of numbers and the potential for inaccuracies when performing mathematical operations. As an alternative, we will use upper and lower bounds for all relevant quantities, and propagate these bounds by rounding up or down as necessary to account for errors introduced by the computer during the calculation process.

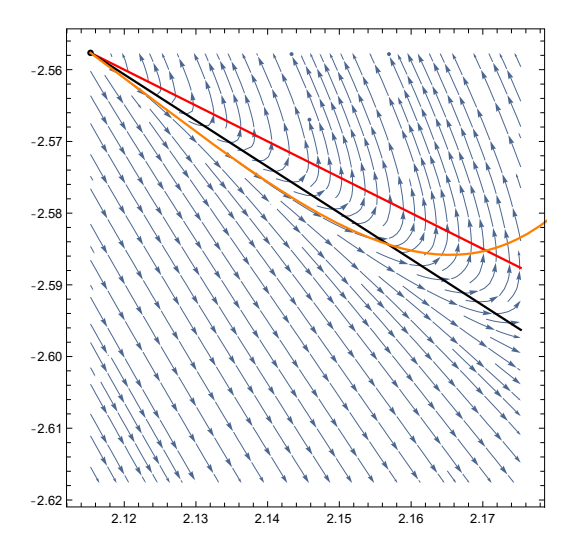


Figure 6: A plot of the vector field (W_{ψ}, Z_{ψ}) for $r = 1.1347 \in (r_3, r_4)$ (moreover $1.1347 \approx r_4$). In the center we have P_s , which is the intersection of $D_Z = 0$ (red line) and $N_Z = 0$ (black curve). We also show $b_4^{\rm nr}(t)$ in orange, for $\beta = 500$.

We can now construct an arithmetic by the theoretic-set definition

$$[x] \star [y] = \{x \star y | \quad x \in [x], y \in [y]\},$$

for any operation $\star \in \{+,-,\times,/\}.$ These are defined by the following equations:

$$\begin{split} [x] + [y] &= [\nabla(\underline{x} + \underline{y}), \Delta(\overline{x} + \overline{y})], \quad [x] - [y] = [\nabla(\underline{x} - \overline{y}), \Delta(\overline{x} - \underline{y})], \\ [x] \times [y] &= [\nabla(\min\{\underline{x}\underline{y}, \underline{x}\overline{y}, \overline{x}\underline{y}, \overline{x}\overline{y}\}), \Delta(\max\{\underline{x}\underline{y}, \underline{x}\overline{y}, \overline{x}\underline{y}, \overline{x}\overline{y}\})], \\ [x] / [y] &= [x] \times \left[\frac{1}{\overline{y}}, \frac{1}{y}\right], \text{ whenever } 0 \notin [y], \end{split}$$

where ∇ and Δ are respectively the round-down and round-up operators.

The main feature of the arithmetic is that if $x \in [x], y \in [y]$, then necessarily $x \star y \in [x] \star [y]$ for any operator \star . This property is fundamental in order to ensure that the true result is always contained in the interval we get from the computer. This process is completely rigorous and independent of the architecture or the software of the computer. We can also define functions of intervals f([x]). For example, if $f([x]) = [x] \times [x] + [x]$, then $f([-1,2]) = [-1,2] \times [-1,2] + [-1,2] = [-2,4] + [-1,2] = [-3,6]$.

Early computer-assisted proofs were constrained to finite dimensional problems [27, 54]; however, recent advances in computational power have enabled the methods to be adapted to infinite dimensional problems (PDE). In the context of fluid mechanics we highlight the following equations: De Gregorio [14], SQG [13], Whitham [26], Muskat [33, 22], Kuramoto-Shivasinsky [3, 28, 30, 29, 59, 60], Navier-Stokes [56, 2], Burgers-Hilbert [24] or the Hou-Luo model [15]. We also refer the reader to the books [48, 55] and to the survey [32] and the book [49] for a more specific treatment of computer-assisted proofs in PDE.

In the paper [7], interval arithmetic is used to check the validity (positivity conditions) of the barriers and to compute a few thousands of coefficients of the Taylor expansion at P_s (the latter is only used for the case $\gamma = \frac{7}{5}$). We performed the rigorous computations using the Arb library [35] and specifically its C

implementation. The positivity checks involve using a branch and bound algorithm to evaluate the open conditions mentioned in the paper. We start by enclosing the condition within a box in a parameter space (which is at most 2-dimensional). If the enclosure provides a definite sign, we accept or reject it based on whether the sign matches the desired result. If the enclosure does not provide a sign, we split the box in half along one of the dimensions and repeat the process. This procedure continues until the maximum length in any dimension of the box reaches a tolerance of 10^{-10} , at which point the program will fail. In our case, this tolerance was never reached.

Acknowledgements

T.B. was supported by the NSF grants DMS-2243205 and DMS-1900149, a Simons Foundation Mathematical and Physical Sciences Collaborative Grant and a grant from the Institute for Advanced Study. G.C.-L. was supported by a grant from the Centre de Formació Interdisciplinària Superior, a MOBINT-MIF grant from the Generalitat de Catalunya and a Praecis Presidential Fellowship from the Massachusetts Institute of Technology. G.C.-L. would also like to thank the Department of Mathematics at Princeton University for partially supporting him during his stay at Princeton and for their warm hospitality. This project has received funding from the European Research Council (ERC) under the European Union's Horizon 2020 research and innovation program through the grant agreement 852741 (G.C.-L. J.G.-S.). J.G.-S. was partially supported by NSF through Grant DMS-1763356 and by the AGAUR project 2021-SGR-0087 (Catalunya). J.G.-S. and G.C.-L. were partially supported by MICINN (Spain) research grant number PID2021–125021NA–100.

References

- [1] Leo Abbrescia and Jared Speck. The emergence of the singular boundary from the crease in 3D compressible Euler flow. $arXiv\ e\text{-}prints$, page arXiv:2207.07107, July 2022.
- [2] Gianni Arioli, Filippo Gazzola, and Hans Koch. Uniqueness and bifurcation branches for planar steady Navier-Stokes equations under Navier boundary conditions. *Journal of Mathematical Fluid Mechanics*, 23, 2021. Article 49.
- [3] Gianni Arioli and Hans Koch. Computer-assisted methods for the study of stationary solutions in dissipative systems, applied to the Kuramoto-Sivashinski equation. Arch. Ration. Mech. Anal., 197(3):1033– 1051, 2010.
- [4] Anxo Biasi. Self-similar solutions to the compressible Euler equations and their instabilities. *Commun. Nonlinear Sci. Numer. Simul.*, 103:Paper No. 106014, 28, 2021.
- [5] Alberto Bressan. Global solutions of systems of conservation laws by wave-front tracking. *J. Math. Anal. Appl.*, 170(2):414–432, 1992.
- [6] Alberto Bressan. The unique limit of the Glimm scheme. Archive for Rational Mechanics and Analysis, 130(3):205–230, 1995.

- [7] Tristan Buckmaster, Gonzalo Cao-Labora, and Javier Gómez-Serrano. Smooth imploding solutions for 3D compressible fluids. *Arxiv preprint arXiv:2208.09445*, 2022.
- [8] Tristan Buckmaster, Theodore Drivas, Steve Shkoller, and Vlad Vicol. Formation and development of singularities for the compressible Euler equations. *Proceedings of the International Congress of Mathematicians*.
- [9] Tristan Buckmaster, Theodore D. Drivas, Steve Shkoller, and Vlad Vicol. Simultaneous Development of Shocks and Cusps for 2D Euler with Azimuthal Symmetry from Smooth Data. Ann. PDE, 8(2):Paper No. 26, 2022.
- [10] Tristan Buckmaster, Steve Shkoller, and Vlad Vicol. Formation of shocks for 2D isentropic compressible Euler. Comm. Pure Appl. Math., 75(9):2069–2120, 2022.
- [11] Tristan Buckmaster, Steve Shkoller, and Vlad Vicol. Formation of point shocks for 3D compressible Euler. *Communications on Pure and Applied Mathematics*, to appear.
- [12] Tristan Buckmaster, Steve Shkoller, and Vlad Vicol. Shock formation and vorticity creation for 3d Euler. Communications on Pure and Applied Mathematics, to appear.
- [13] Angel Castro, Diego Córdoba, and Javier Gómez-Serrano. Global smooth solutions for the inviscid SQG equation. *Memoirs of the AMS*, 266(1292):89 pages, 2020.
- [14] Jiajie Chen, Thomas Y. Hou, and De Huang. On the Finite Time Blowup of the De Gregorio Model for the 3D Euler Equations. *Communications on Pure and Applied Mathematics*, 74(6):1282–1350, 2021.
- [15] Jiajie Chen, Thomas Y. Hou, and De Huang. Asymptotically self-similar blowup of the Hou-Luo model for the 3D Euler equations. *Ann. PDE*, 8(2):Paper No. 24, 75, 2022.
- [16] Shuxing Chen and Liming Dong. Formation and construction of shock for p-system. Sci. China Ser. A, 44(9):1139–1147, 2001.
- [17] R. F. Chisnell. An analytic description of converging shock waves. *Journal of Fluid Mechanics*, 354:357–375, 1998.
- [18] Demetrios Christodoulou. *The formation of shocks in 3-dimensional fluids*. EMS Monographs in Mathematics. European Mathematical Society (EMS), Zürich, 2007.
- [19] Demetrios Christodoulou. The shock development problem. EMS Monographs in Mathematics. European Mathematical Society (EMS), Zürich, 2019.
- [20] Demetrios Christodoulou and André Lisibach. Shock development in spherical symmetry. Ann. PDE, 2(1):Art. 3, 246, 2016.
- [21] Demetrios Christodoulou and Shuang Miao. Compressible flow and Euler's equations, volume 9 of Surveys of Modern Mathematics. International Press, Somerville, MA; Higher Education Press, Beijing, 2014.

- [22] Diego Córdoba, Javier Gómez-Serrano, and Andrej Zlatoš. A note on stability shifting for the Muskat problem, II: From stable to unstable and back to stable. *Anal. PDE*, 10(2):367–378, 2017.
- [23] Constantine M. Dafermos. Hyperbolic conservation laws in continuum physics, volume 325 of Grundlehren der Mathematischen Wissenschaften [Fundamental Principles of Mathematical Sciences]. Springer-Verlag, Berlin, third edition, 2010.
- [24] Joel Dahne and Javier Gómez-Serrano. Highest cusped waves for the Burgers-Hilbert equation. ArXiv preprint arXiv:2205.00802, 2022.
- [25] Ronald J. DiPerna. Global solutions to a class of nonlinear hyperbolic systems of equations. *Comm. Pure Appl. Math.*, 26:1–28, 1973.
- [26] Alberto Enciso, Javier Gómez-Serrano, and Bruno Vergara. Convexity of cusped Whitham waves. Arxiv preprint arXiv:1810.10935, 2018.
- [27] C. Fefferman and R. de la Llave. Relativistic stability of matter. I. Rev. Mat. Iberoamericana, 2(1-2):119–213, 1986.
- [28] Jordi-Lluís Figueras and Rafael de la Llave. Numerical computations and computer assisted proofs of periodic orbits of the Kuramoto-Sivashinsky equation. SIAM J. Appl. Dyn. Syst., 16(2):834–852, 2017.
- [29] Jordi-Lluís Figueras, Marcio Gameiro, Jean-Philippe Lessard, and Rafael de la Llave. A framework for the numerical computation and a posteriori verification of invariant objects of evolution equations. SIAM J. Appl. Dyn. Syst., 16(2):1070–1088, 2017.
- [30] Marcio Gameiro and Jean-Philippe Lessard. A posteriori verification of invariant objects of evolution equations: periodic orbits in the Kuramoto-Sivashinsky PDE. SIAM J. Appl. Dyn. Syst., 16(1):687–728, 2017.
- [31] James Glimm. Solutions in the large for nonlinear hyperbolic systems of equations. *Communications on Pure and Applied Mathematics*, 18(4):697–715, 1965.
- [32] Javier Gómez-Serrano. Computer-assisted proofs in PDE: a survey. SeMA J., 76(3):459–484, 2019.
- [33] Javier Gómez-Serrano and Rafael Granero-Belinchón. On turning waves for the inhomogeneous Muskat problem: a computer-assisted proof. *Nonlinearity*, 27(6):1471–1498, 2014.
- [34] G. Guderley. Starke kugelige und zylindrische Verdichtungsstösse in der Nähe des Kugelmittelpunktes bzw. der Zylinderachse. *Luftfahrtforschung*, 19:302–311, 1942.
- [35] F. Johansson. Arb: efficient arbitrary-precision midpoint-radius interval arithmetic. IEEE Transactions on Computers, 66:1281–1292, 2017.
- [36] Fritz John. Formation of singularities in one-dimensional nonlinear wave propagation. Comm. Pure Appl. Math., 27:377–405, 1974.

- [37] De-Xing Kong. Formation and propagation of singularities for 2×2 quasilinear hyperbolic systems. Trans. Amer. Math. Soc., 354(8):3155-3179, 2002.
- [38] L. D Landau and E. M Lifshitz. Fluid Mechanics: Volume 6. Elsevier Science, 1987. OCLC: 936858705.
- [39] Peter D. Lax. Development of singularities of solutions of nonlinear hyperbolic partial differential equations. J. Mathematical Phys., 5:611–613, 1964.
- [40] M.-P. Lebaud. Description de la formation d'un choc dans le p-système. J. Math. Pures Appl. (9), 73(6):523–565, 1994.
- [41] T. P. Liu. Development of singularities in the nonlinear waves for quasilinear hyperbolic partial differential equations. *J. Differential Equations*, 33(1):92–111, 1979.
- [42] Jonathan Luk and Jared Speck. Shock formation in solutions to the 2D compressible Euler equations in the presence of non-zero vorticity. *Invent. Math.*, 214(1):1–169, 2018.
- [43] Jonathan Luk and Jared Speck. The stability of simple plane-symmetric shock formation for 3D compressible Euler flow with vorticity and entropy. *Analysis and PDE*, 2021. To appear.
- [44] A. Majda. The existence of multidimensional shock fronts. *Mem. Amer. Math. Soc.*, 43(281):v+93, 1983.
- [45] Frank Merle, Pierre Raphaël, Igor Rodnianski, and Jeremie Szeftel. On blow up for the energy super critical defocusing nonlinear Schrödinger equations. *Invent. Math.*, 227(1):247–413, 2022.
- [46] Frank Merle, Pierre Raphaël, Igor Rodnianski, and Jeremie Szeftel. On the implosion of a compressible fluid I: smooth self-similar inviscid profiles. *Ann. of Math.* (2), 196(2):567–778, 2022.
- [47] Frank Merle, Pierre Raphaël, Igor Rodnianski, and Jeremie Szeftel. On the implosion of a compressible fluid II: singularity formation. *Ann. of Math.* (2), 196(2):779–889, 2022.
- [48] R.E. Moore and F. Bierbaum. *Methods and applications of interval analysis*, volume 2. Society for Industrial & Applied Mathematics, 1979.
- [49] Mitsuhiro T. Nakao, Michael Plum, and Yoshitaka Watanabe. Numerical Verification Methods and Computer-Assisted Proofs for Partial Differential Equations, volume 53 of Springer Series in Computational Mathematics. Springer, Singapore, 2019.
- [50] Olga Rozanova. Blow-up of smooth highly decreasing at infinity solutions to the compressible Navier–Stokes equations. *Journal of Differential Equations*, 245(7):1762–1774, 2008.
- [51] Steve Shkoller and Vlad Vicol. Maximal development for Euler shock formation. preprint, 2022.
- [52] Thomas C. Sideris. Delayed singularity formation in 2D compressible flow. *Amer. J. Math.*, 119(2):371–422, 1997.

- [53] J. Meyer ter Vehn and C. Schalk. Selfsimilar spherical compression waves in gas dynamics. Zeitschrift für Naturforschung A, 37(8):954–970, August 1982.
- [54] Warwick Tucker. A rigorous ODE solver and Smale's 14th problem. Found. Comput. Math., 2(1):53–117, 2002.
- [55] Warwick Tucker. Validated numerics. Princeton University Press, Princeton, NJ, 2011. A short introduction to rigorous computations.
- [56] Jan Bouwe van den Berg, Maxime Breden, Jean-Philippe Lessard, and Lennaert van Veen. Spontaneous periodic orbits in the Navier–Stokes flow. *Journal of Nonlinear Science*, 31, 2021. Article 41.
- [57] Zhouping Xin. Blowup of smooth solutions to the compressible Navier-Stokes equation with compact density. Communications on Pure and Applied Mathematics, 51(3):229–240, 1998.
- [58] Huicheng Yin. Formation and construction of a shock wave for 3-D compressible Euler equations with the spherical initial data. Nagoya Math. J., 175:125–164, 2004.
- [59] Piotr Zgliczyński. Rigorous Numerics for Dissipative Partial Differential Equations II. Periodic orbit for the Kuramoto-Sivashinsky PDE—a Computer-Assisted Proof. Found. Comput. Math., 4(2):157–185, 2004.
- [60] Piotr Zgliczyński and Konstantin Mischaikow. Rigorous Numerics for Partial Differential Equations: The Kuramoto-Sivashinsky equation. *Found. Comput. Math.*, 1(3):255–288, 2001.